Optik - International Journal for Light and Electron Optics 244 (2021) 166324

Contents lists available at ScienceDirect

Optik

journal homepage: www.elsevier.com/locate/ijleo

Original research article

Halogens effect on spectroscopy, anticancer and molecular docking studies for platinum complexes

Hunar Hama Khalid [a], Sultan Erkan [b,*], Niyazi Bulut [a]

[a] Department of Physics, Faculty of Science, Firat University, Elazig, Turkey
[b] Department of Chemistry, Faculty of Science, Sivas Cumhuriyet University, Sivas, Turkey

ARTICLE INFO

Keywords:
Platinum complexes
FTIR
NMR
Molecular docking
Anti-cancer

ABSTRACT

Pt(dpb)Cl, Pt(Fdpb)Cl, Pt(F_2dpb)Cl and Pt(dpb)I complexes are examined by computational chemistry method in all aspects. Hartree-Fock (HF) and Density Functional Theory (DFT) methods at B3LYP and M062X level of functions with CEP-4G, CEP-31G, CEP-12G, LANL2DZ, LANL2MB, and SDD basis sets are used in calculation to obtain an optimal level. Spectral analysis (^{1}H-NMR, ^{13}C-NMR, IR and Emission) calculations are reported and compared with the available experimentally data. To discuss activities of the systems at a molecular level, pharmaceutically active four platinum complexes were studied. In addition, biological activity studies of the complexes have been done by using a molecular docking support and finally emission spectra and OLED properties of platinum complexes were examined. For the first time it was found that platinum complexes may have some photoactive chemotherapeutic properties and can be considered as an anticancer drugs.

1. Introduction

Addition of light in cancer treatment has led to some new developments in the design of anticancer drugs [1]. A compound that reacts to light is a photoactive chemotherapeutic (PACT) drug candidate used in chemotherapy. The photoactive drug is selectively activated by photo-irradiation to kill cancer cells [2–4]. Cytotoxic species can be produced in a controlled manner by activation of metal complexes in PACTs. Photoinduced electron transfer causes the ligand to metal charge transfer (LMCT) transitions in low-spin metal complexes. These transitions lead to electron transition from ligand to metal and/or ligand decomposition [5]. The therapeutic effect can be explained by the reduction of metal complexes or with the ligand released or both. In any case, the final form of the complex may interact with DNA and other biomolecules. Furthermore, light irradiation causes the complexes to emit irradiation and to generate an excited metal-to-ligand charge-transfer triplet state (MLCT). This MLCT state rapidly undergoes an internal transformation by becoming a metal-centered triple-state (MC). Likewise, this contributes to the formation of reactive species with the therapeutic effect by the release of a ligand or the release of the metal or both [6].

Pt(II) complexes were evaluated with respect to cell growth inhibition against different types of human cancer cell lines [16]. They possess a number of distinctive characteristics, such as a broad spectrum of emission colors, elevated luminescence quantity, brief lifetime of triplet excited states [17]. Shinozaki et al. reported the effects of Pt(dpb)Cl (dpbH = 1,3-di(2-pyridyl)benzene), Pt(Fdpb)Cl (FdpbH = 4-fluoro-1,3-di(2-pyridyl)benzene), Pt(F_2dpb)Cl (F_2dpbH = 4,6-difluoro-1,3-di(2-pyridyl)benzene) and Pt(dpb)I on the

* Corresponding author.
E-mail address: sultanerkan58@gmail.com (S. Erkan).

https://doi.org/10.1016/j.ijleo.2021.166324
Received 26 November 2020; Accepted 14 January 2021
Available online 22 January 2021
0030-4026/

excimer emission of the solvent and the substituent. In their study it has been shown that the Pt(II) complex can be found not only as a blue-green emitter as monomer, but also as red and NIR emitters as excimer and trimer and also they suggested that Pt(N^C^N)Cl could be a potentially sensing luminophore to report the lipid layer, micelle, living cell, and similar microenvironments [9].

In this study, spectroscopic and anticancer properties of Pt (II) complexes bearing a dpb ligand shown in Scheme 1 are investigated depending on the molecular structure.

2. Theoretical calculations

The input files of relevant complexes were prepared with GaussView 5.0.8 [10]. All data are obtained in the package Gaussian IA32W-G09RevA.02 and Gaussian AS64L-G09RevD.01 [11,12]. A benchmark analysis was performed with the HF [13] and DFT methods (B3LYP [14,15] and M062X [16]) and basis sets (CEP-4G, CEP-31G, CEP-12G [17], LANL2DZ [18], LANL2MB [19], and SDD [19]) using experimental ^{1}H-NMR chemical shift data of the Pt(dpb)Cl, Pt(Fdpb)Cl, Pt(F_2dpb)Cl and Pt(dpb)I complexes. The most appropriate calculation level was found as M062X/CEP-31G according to the proximity of one of the calculated and experimental result.

3. Result and discussion

3.1. Benchmark analyses

Before start to calculate any quantities with a computational chemistry method someone needs to optimize molecular structure with respect to energy minimizing. During that minimizing it is also important to obtain and interpret regression coefficients giving us some idea between theoretical deviation in respect to experimental one. The regression coefficients results obtained with HF, B3LYP, M062X methods at CEP-4G, CEP-31G, CEP-12G, LANL2DZ, LANL2MB, SDD level of basis sets in comparison with the experimental data are listed in Table 1. For this purpose, HF, B3LYP, M062X methods and CEP-4G, CEP-31G, CEP-12G, LANL2DZ, LANL2MB, SDD basis sets and proton chemical shift values were calculated for the Pt(dpb)I complex. Firstly, atomic labeling of the Pt(dpb)I complex is given in Fig. 1. Then, the calculated and the experimental 1H-NMR chemical shift values for the Pt(dpb)I complex are given in Table 1–3.

The regression coefficients results obtained with HF, B3LYP, M062X methods at CEP-4G, CEP-31G, CEP-12G, LANL2DZ, LANL2MB, SDD level of basis sets in comparison with the experimental data are listed in Table 4.

These coefficients provide the ratio of the variance between one variable and the other. When R^2 values taken into account, it is closer to 1 for the M062X/CEP-31G level as can be seen in the last column of Table 4. This is one of the reasons chosen M062X/CEP-31G basis set for all rest of quantum calculations in this study. To interpret proton chemical shift, tetra methyl silane (TMS) was taken as a reference. ^{1}H-NMR values of TMS was calculated for all methods and basis sets. The chemical shift for TMS proton was found to be 32.78 ppm at the M062X/CEP-31G level. Calculated chemical shift values for Pt(dpb)I are 10.92, 9.12, 9.04, 8.95, 8.88 and 8.86 ppm and experimental values corresponding to the calculated chemical shifts are 9.83, 8.18, 8.05, 7.71, 7.48 and 7.38 ppm for Pt(dpb)I complex [9].

3.2. Optimized structure

The optimized structure of Pt(dpb)Cl, Pt(Fdpb)Cl, Pt(F_2dpb)Cl and Pt(dpb)I were picturized in Fig. 1. Considering the geometry structure of all complexes, the tridentate 1,3-di(2-pyridyl) phenyl and halogen ligands formed a square planar geometry around the platinum as can be seen in Fig. 1.

3.3. FT-IR Spectra and vibrational assignments

FT-IR spectra is a very important technique in recognition of the skeletal structure of the investigated chemical species. For all complexes harmonic frequencies were calculated at M062X/CEP-31G level. Theoretically simulated IR spectrum of the studied complexes is given in Fig. 2. Bond stretching modes corresponding to the peaks in the IR spectrum of investigated platinum complexes are also given in Table 5 and C—H, C—C, C═C, C—N and C═N bond stretching modes were evaluated in detail in following subsection.

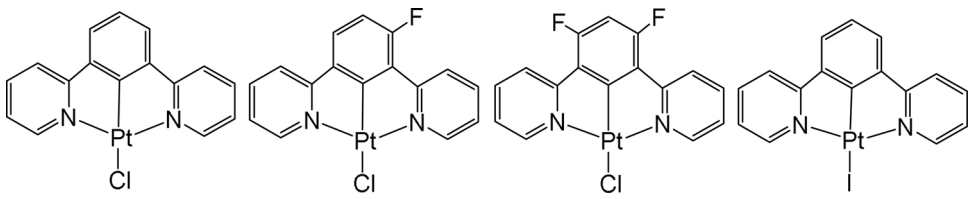

Scheme 1. Structures of Pt(dpb)Cl, Pt(Fdpb)Cl, Pt(F_2dpb)Cl, and Pt(dpb)I.

Table 1
^{1}H-NMR chemical shift values at calculated in GIAO/HF method and the different basis sets in gas phase for Pt(dpb)I (δ = ppm).

Assign.	CEP-4G	CEP-31G	CEP-121G	LANL2DZ	LANL2MB	SDD	Exp.
21 H	11.13	10.29	10.35	10.92	9.95	9.91	9.83
22 H	9.77	8.17	7.86	8.19	7.77	7.20	8.18
23 H	10.49	8.91	8.86	9.07	8.39	8.08	7.48
24 H	10.15	8.60	8.32	8.46	8.01	7.47	8.05
25 H	10.17	8.87	8.58	8.70	7.97	7.67	7.71
26 H	9.32	8.69	7.91	8.05	7.61	6.99	7.38
27 H	8.37	8.87	8.58	8.70	7.97	7.67	7.71
28 H	10.15	8.60	8.32	8.46	8.01	7.47	8.05
29 H	10.49	8.91	8.86	9.07	8.39	8.08	7.48
30 H	9.77	8.17	7.86	8.18	7.77	7.20	8.18
31 H	11.13	10.29	10.35	10.92	9.95	9.91	9.83
Ref.	31.08	33.40	33.45	33.66	33.11	33.66	–

δ=$\Sigma_{H(references)}$-Σ, $\Sigma_{H(reference)\ (gaz)}$, Reference TMS.

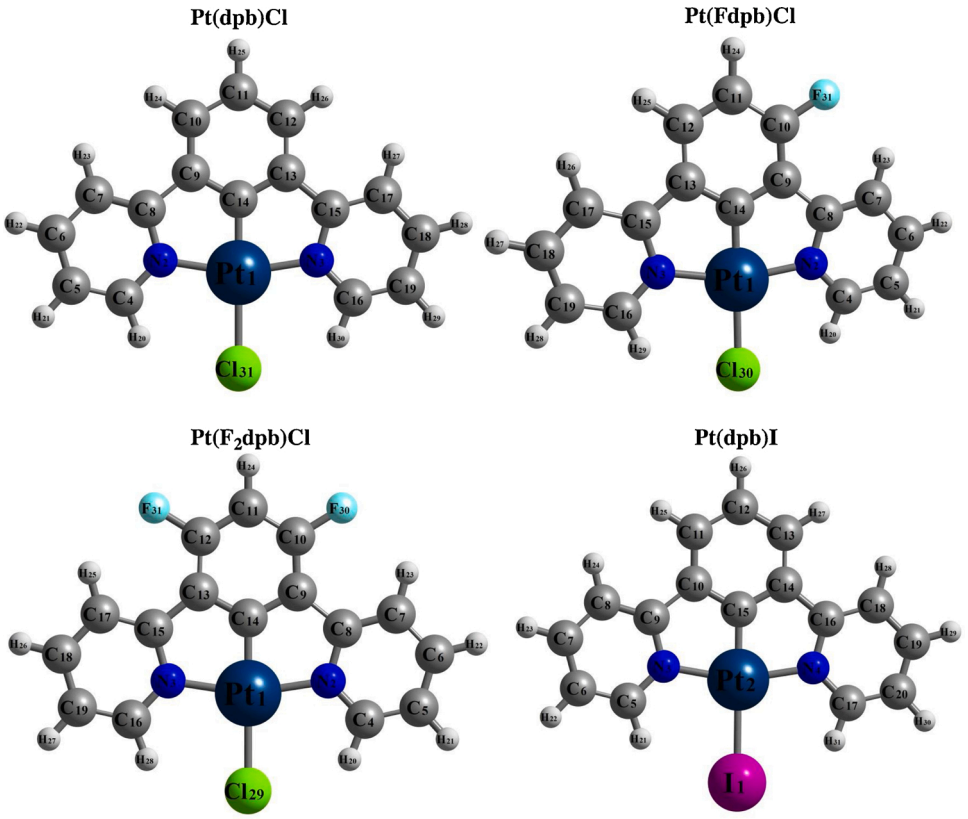

Fig. 1. Optimized structures and atomic labeling for Pt(dpb)Cl, Pt(Fdpb)Cl, Pt(F_2dpb)Cl and Pt(dpb)I.

3.3.1. C—H bond stretching

In aromatic compounds, stretching, in plane bending and out of plane bending CH vibration modes can appear in 3100−3000 cm^{-1}, 1400−1000 cm^{-1}, and 1000−750 cm^{-1} ranges respectively [20,21]. The stretching CH modes are generally appears in a range of 3100−3000 cm^{-1} with multiple soft bands and these bands may not be affected a whole nature of the substituent's [22–25]. The βC—H vibration modes show moderately sharp but not strong bands in the range 1100−1500 cm^{-1} and these bands are not so sensitive to the nature of substituents. The out of plane bending C—H deformation modes in general are in a range of 800–1000 cm-1 [23]. The C—H asymmetric stretching found in a position of 3080 cm^{-1} and the C—H symmetric stretching assigned to 3008, 2982 cm^{-1}. The tighter absorptions for aromatic compounds as can been in the figure occurs in the range of 900–650 cm^{-1} because of the C—H vibrations modes out of the plane to the aromatic ring [26–28]. In present work, the C—H stretching vibration mode is observed at about 3207−3278 cm^{-1} for Pt(dpb)Cl, 3222−3283 cm^{-1} for Pt(Fdpb)Cl, 3242−3282 cm^{-1} Pt(F_2dpb)Cl and 3209−3279 cm^{-1} Pt(dpb)I which are reasonable a range of wave number with the literature. The C—H bending vibrations (in-plane and out-of-plane) are assigned at 1081−1696 cm^{-1}, 1155−1701 cm^{-1}, 1087−1705 cm^{-1}, and 1086−1698 cm^{-1} for Pt(dpb)Cl, Pt

Table 2
^{1}H-NMR chemical shift values at calculated in GIAO/B3LYP method and the different basis sets in gas phase for Pt(dpb)I (δ = ppm).

Assign.	CEP-4G	CEP-31G	CEP-121G	LANL2DZ	LANL2MB	SDD	Exp.
21 H	10.41	10.26	10.15	−1.36	9.27	10.64	9.83
22 H	8.99	7.83	7.44	3.70	7.18	7.70	8.18
23 H	9.18	8.11	7.97	4.00	7.37	8.11	7.48
24 H	9.42	8.31	7.93	−0.74	7.35	7.99	8.05
25 H	9.22	8.25	7.88	3.03	7.09	7.94	7.71
26 H	8.56	7.67	7.39	1.69	6.83	7.46	7.38
27 H	9.22	8.25	7.88	3.03	7.09	7.94	7.71
28 H	9.42	8.31	7.93	−0.75	7.35	7.99	8.05
29 H	9.18	8.11	7.97	4.00	7.37	8.11	7.48
30 H	8.99	7.83	7.44	3.70	7.18	7.70	8.18
31 H	10.41	10.26	10.15	−1.36	9.27	10.64	9.83
Ref.	30.26	32.66	32.71	32.82	32.22	32.76	–

δ=$\Sigma_{H(references)}$-Σ, $\Sigma_{H(reference)\ (gaz)}$, Reference TMS.

Table 3
^{1}H-NMR chemical shift values at calculated in GIAO/M062X method and the different basis sets in gas phase for Pt(dpb)I (δ = ppm).

Assign.	CEP-4G	CEP-31G	CEP-121G	LANL2DZ	LANL2MB	SDD	Exp.
21 H	11.16	10.92	10.90	11.58	10.02	11.42	9.83
22 H	10.08	9.12	8.90	8.83	7.92	8.80	8.18
23 H	10.24	8.88	8.84	8.92	8.12	8.85	7.48
24 H	10.50	9.04	8.78	8.80	8.13	8.75	8.05
25 H	10.15	8.95	8.53	8.79	7.86	8.68	7.71
26 H	9.55	8.86	8.51	8.62	7.59	8.50	7.38
27 H	10.15	8.95	8.53	8.79	7.86	8.68	7.71
28 H	10.50	9.04	8.78	8.80	8.13	8.75	8.05
29 H	10.24	8.88	8.84	8.92	8.12	8.85	7.48
30 H	10.08	9.12	8.90	8.83	7.92	8.80	8.18
31 H	11.16	10.92	10.90	11.58	10.02	11.42	9.83
Ref.	30.53	32.78	32.91	32.96	32.58	32.88	–

δ=$\Sigma_{H(references)}$-Σ, $\Sigma_{H(reference)\ (gaz)}$, Reference TMS.

Table 4
Calculated regression coefficients (R^2) and experimental values for chemical shifts of ^{1}H-NMR.

Basis set	HF	B3LYP	M062X
CEP-4G	0.3821	0.8197	0.7701
CEP-31G	0.6038	0.8538	**0.9520**
CEP-121G	0.6224	0.8125	0.9206
LANL2DZ	0.7032	0.4877	0.8928
LANL2MB	0.7569	0.8918	0.8923
SDD	0.7080	0.8525	0.9028

(Fdpb)Cl, Pt(F_2dpb)Cl, and Pt(dpb)I, respectively and are listed in Table 5.

3.3.2. C═C, C—C bond stretching vibrations

In general, C—C stretching vibrations modes in aromatic compounds can form a band in the estimation region of 1430–1650 cm^{-1} [29]. The ring of C—C stretching vibrations in Pyridine are reported in literature as 1329–1431, 1420–1501 and 1419−1519 cm^{-1}, respectively [30,31]. The computed wavenumber for ν(C—C) modes falls between 1314−1696 cm^{-1}, 1316−1701 cm^{-1}, 1314−1705 cm^{-1}, 1315−1698 cm^{-1} for Pt(dpb)Cl, Pt(Fdpb)Cl, Pt(F_2dpb)Cl, and Pt(dpb)I, respectively.

3.3.3. C═N, C—N bond stretching

One of the difficult task is to obtaining of C═N and C—N vibrations modes, for some mixing of vibrations can be possible in this region. C═N and C—N stretching vibrations appears in a range of 1670−1600 cm^{-1} and 1382−1266 cm^{-1} respectively [32]. The C═N and stretching vibrations of the title compounds lies at 1639, 1644 cm^{-1}, 1639, 1645 cm^{-1}, 1641, 1646 cm^{-1}, 1640, 1645 cm^{-1}, for Pt(dpb)Cl, Pt(Fdpb)Cl, Pt(F_2dpb)Cl, and Pt(dpb)I, respectively.

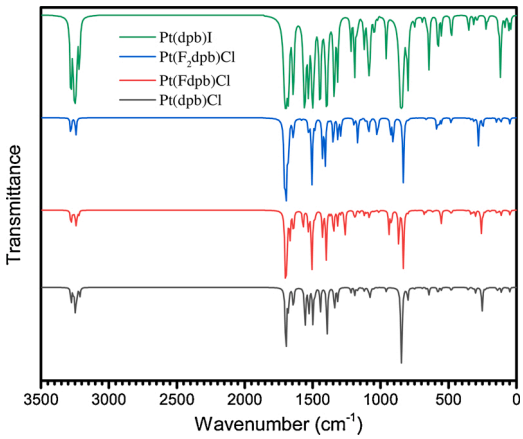

Fig. 2. FT-IR spectra of Pt(dpb)Cl, Pt(Fdpb)Cl, Pt(F_2dpb)Cl, and Pt(dpb)I.

Table 5
Calculated vibrational frequencies (cm^{-1}) of Pt(dpb)Cl, Pt(Fdpb)Cl, Pt(F_2dpb)Cl, and Pt(dpb)I.

Modes	Pt(dpb)Cl	Pt(Fdpb)Cl	Pt(F_2dpb)Cl	Pt(dpb)I
Γ C—H	799 (vw)	833 (vs)	833 (vs)	798 (vw)
ΓC—H	846 (vs)	866 (m)	905 (vw)	847 (vs)
ΓC—H	958 (vw)	920 (vw)	926 (w)	958 (vw)
βC—H	1080 (vw)	1155 (vw)	1087 (w)	1086 (vw)
βC—H	1190 (vw)	1264 (m)	1168 (m)	1191 (vw)
βC—H	1314 (vw)	1344 (vw)	1293 (m)	1341 (w)
βC—H	1337 (vw)	1400 (s)	1407 (s)	1396 (s)
βC—H	1394 (s)	1506 (s)	1427 (m)	1445 (m)
βC—H	1498 (m)	1570 (w)	1505 (vs)	1499 (s)
βC—H	1555 (m)	1688 (m)	1677 (m)	1558 (m)
βC—H	1644 (vw)	1696 (vs)	1696 (vs)	1645 (vw)
βC—H	1696 (vs)	1701 (m)	1705 (vs)	1698 (vs)
νC—H	3214 (vw)	3222 (vw)	3242 (vw)	3209 (vw)
νC—H	3238 (vw)	3241 (vw)	3276 (vw)	3239 (vw)
νC—H	3247 (vw)	3275 (vw)	3281 (vw)	3248 (w)
νC—H	3278 (vw)	3283 (vw)	3282 (vw)	3279 (w)
νC═C	1314 (vw)	1316 (vw)	1315 (w)	1315 (vw)
νC═C	1394 (s)	1400 (s)	1407 (s)	1396 (s)
νC═C	1442 (m)	1427 (m)	1427 (m)	1445 (m)
νC═C	1498 (m)	1570 (w)	1505 (vs)	1499 (s)
νC═C	1528 (m)	1639 (vw)	1641 (vw)	1531 (w)
νC═C	1555 (m)	1667 (m)	1677 (m)	1558 (m)
νC═C	1644 (vw)	1688 (m)	1691 (m)	1645 (vw)
νC═C	1678 (m)	1696 (vs)	1696 (vs)	1679 (w)
νC═C	1696 (vs)	1701 (m)	1705 (vs)	1698 (vs)
C—N	1314 (w)	1316 (vw)	1314 (w)	1315 (vw)
C═N	1639 (w)	1639 (vw)	1641 (vw)	1640 (vw)
C═N	1644 (w)	1645 (vw)	1646 (vw)	1645 (vw)

ν: Stretching, β: in-plane-bending, Γ: out-of-plane bending, vw: very week, w: week, m: medium, s: strong, vs: very strong.

3.4. NMR spectra

Nuclear magnetic resonance (NMR) is a popular technique to characterize any complex macromolecules [33]. DFT methods for calculations of magnetic shielding highly extends the size of molecules [34,35]. Electronegative groups close to the system reduce the surrounding electron density, shielding of peak position from the external magnetic field and moving the signal to higher ppm. Intermolecular effects can be examined by chemical shifts and this examination show how electron density and electronegativity of neighboring groups influence the chemical shift observed for the molecule. A plotting comparative of calculated ^{13}C-NMR chemical shifts calculated at M062X/CEP-31G level of studied complexes is given in Fig. 3. In addition, the calculated chemical shift values (δ_C) of carbons in the complexes are given in Table 6.

The ^{13}C NMR spectrum of considered molecules as can be seen from Fig. 3 shows some sharp peaks corresponding to various carbon atoms because of the non-equivalence of the various carbon atoms. From Fig. 3 one can notice that in Pt(dpb)Cl, Pt(F_2dpb)Cl, Pt(dpb)I cases there are almost intense peaks by overlapping peak positions, but in a case Pt(Fdpb)Cl it can be see just one intense peak occurs

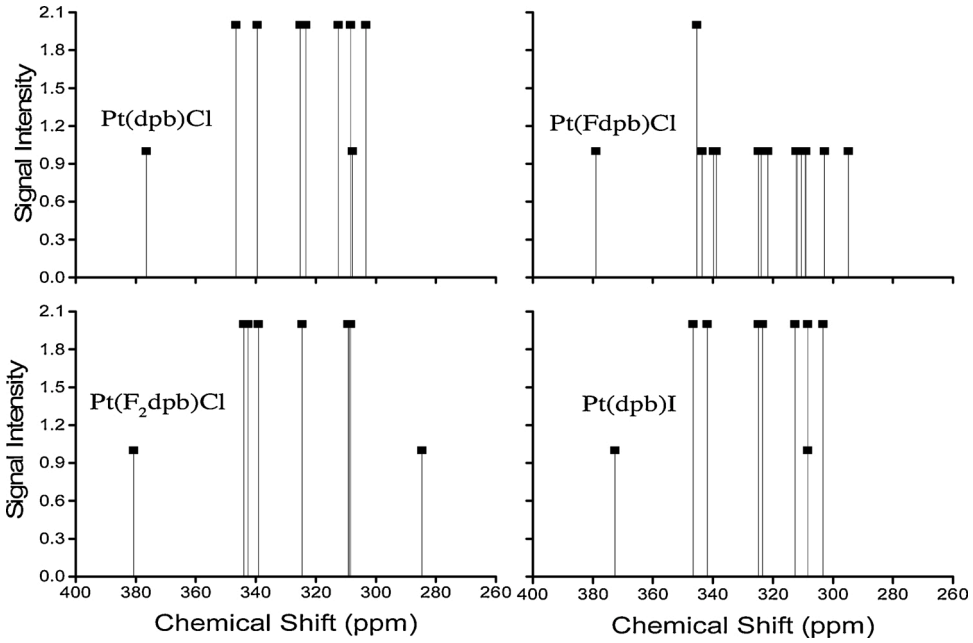

Fig. 3. ^{13}C-NMR spectra of mentioned complexes.

Table 6
Experimental and calculated ^{13}C-NMR chemical shift (ppm) for mentioned complexes.

Pt(dpb)Cl		Pt(Fdpb)Cl		Pt(F_2dpb)Cl		Pt(dpb)I	
Atoms	δ_{calc}	Atoms	δ_{calc}	Atoms	δ_{calc}	Atoms	δ_{calc}
14C	376	14C	378	14C	380	15C	372
15C	346	10C	345	12C	344	9C	346
8C	346	15C	345	10C	344	16C	346
16C	339	8C	343	8C	342	17C	341
4C	339	16C	339	15C	342	5C	341
13C	325	4C	338	16C	339	10C	324
9C	325	6C	324	4C	339	14C	324
6C	323	18C	323	18C	324	7C	323
18C	323	13C	321	6C	324	19C	323
10C	312	12C	312	5C	309	13C	312
12C	312	9C	311	19C	309	11C	312
5C	308	5C	310	13C	308	12C	308
19C	308	19C	309	9C	308	20C	308
11C	307	7C	309	7C	308	6C	308
7C	303	17C	302	17C	308	18C	303
17C	303	11C	294	11C	284	8C	303

because of losing symmetry of the system. The efficiency of the electronegative, however, is dependent upon far-near and direct-indirect interactions between the electronegative atoms and its neighboring carbons. As seen in Table 3, generally similar ^{13}C-NMR chemical shifts were obtained as the complexes were similar molecular structures. Platinum bonded C14 chemical shifts were calculated in the range 372−380 ppm. The highest ^{13}C-NMR chemical shift belongs to these carbons. This is because the C14 s are less shielded by the central atom. In addition, carbons with neighboring nitrogen are also exhibited high chemical shifts. 13C-NMR chemical shifts of these carbons are in the range of 339−346 ppm. The calculation results support theoretical expectations.

Because the electronegative nitrogen atom attracts more electrons from adjacent α-carbons. This is results in less shielding of the carbon cores. Less shielded carbons exhibit greater chemical shift values than other carbon atoms in the ring. A similar situation is observed in the fluorine bound carbons in Pt(Fdpb)Cl and Pt(F_2dpb)Cl complexes.

3.5. Molecular electrostatic potential (MEP) surface

To have a deeply interpretation of reactivity of any molecule, electrostatic potential calculations may give some advantage to evaluate the reactivity of molecules against positively or negatively charged reactants. Molecular electrostatic potential surface calculated and are depicted in Fig. 4. In this figure the high-density parts of the electrostatic potential energy values are colored with

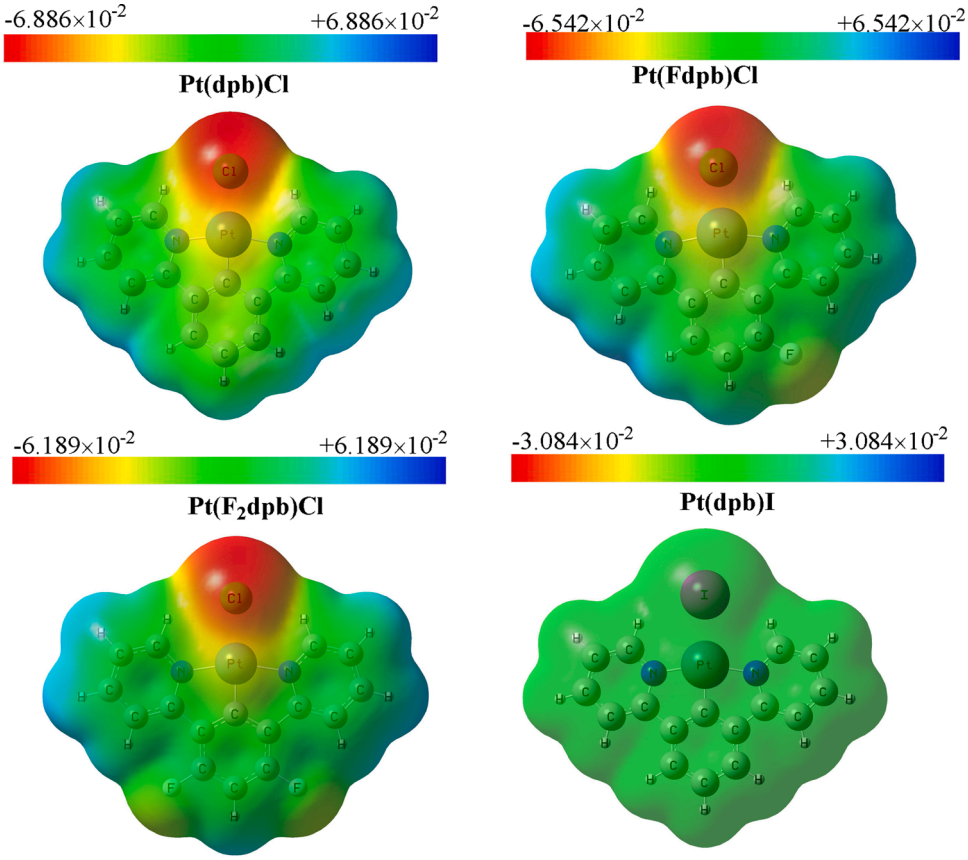

Fig. 4. The molecular electrostatic potential (MEP) surface maps for Pt(dpb)Cl, Pt(Fdpb)Cl, Pt(F_2dpb)Cl and Pt(dpb)I complexes.

red and the lowest part is blue [36].

As can be seen from Fig. 4, the active zones of the MEP, which is colored with red, of the complexes Pt(dpb)Cl, Pt(Fdpb)Cl, Pt (F_2dpb) Cl are the regions where the chlorine atom is located. When the ESP load densities are examined, the ESP charge for Pt(dpb)Cl, Pt(Fdpb)Cl, Pt(F_2dpb)Cl are $\pm 6.886 \times 10^{-2}$, $\pm 6.542 \times 10^{-2}$ and $\pm 6.189 \times 10^{-2}$, respectively. The ESP charge density for Pt(dpb)I is $\pm 3.084 \times 10^{-2}$. This may show that the Pt(dpb)I complex has an electropositive region. Considering these values and MEP figures one concludes that Chlorine complexes may interact with cancer cells more than iodine complex. Also, MEP maps can be predicted from which region the complexes interact actively with cancer cells.

3.6. Molecular docking study

Platinum-based complexes are widely used in treatment of almost all types of cancer such as breast, ovarian, colon, pancreatic, lung, melanoma. Molecular docking study for Pt(F_2dpb)Cl, Pt(Fdpb)Cl, Pt(dpb)Cl, and Pt(dpb)I were performed with PDB ID:1JNX [37] (crystal structure of breast cancer-associated protein BRCT), PDB ID:1X2J [38] (structural basis of defects in point mutations on the lung cancer), PDB ID:2VFJ [39] (structure of the A20 ovarian tumor domain), PDB ID:4J80 [40] (crystal structures of the multidomain cochaperone DnaJ on the pancreatic cancer), PDB ID:4ZQK [41] (Structure of the complex of human programmed on the non-small cell lung cancer). Optimized structures of Pt(F_2dpb)Cl, Pt(Fdpb)Cl, Pt(dpb)Cl, and Pt(dpb)I were transformed into pdb files with GaussView 6.0 program. 1JNX, 1X2J, 2VFJ, 4J80 and 4ZQK target proteins were procurement in the protein data bank. HEX 8.0.0 program [42] and Docking Server [43] was used to obtain the binding energies of related complexes with the target proteins. The

Table 7
The interaction energies between studied proteins and the selected target proteins.

Target protein	Pt(F_2dpb)Cl	Pt(Fdpb)Cl	Pt(dpb)Cl	Pt(dpb)I	Cis-Pt
1JNX	−262.81	−252.93	−247.41	−256.93	−122.27
1X2J	−262.86	−257.27	−253.30	−255.34	−120.73
2VFJ	−17.13	−19.26	−13.49	−16.79	−25.47
4J80	−22.43	−19.74	−15.64	−27.76	−21.30
4ZQK	−243.69	−229.87	−235.10	−234.30	−121.69

binding energies between Pt(F_2dpb)Cl, Pt(Fdpb)Cl, Pt(dpb)Cl, and Pt(dpb)I with 1JNX, 1X2J, 2VFJ, 4J80 and 4ZQK were given Table 7.

Cis-platinum is a complex and widely used in cancer treatment. This complex, generally, is taken as a reference and the efficacy of newly discovered platinum complexes is investigated for interaction energies of Pt(F2dpb)Cl, Pt(Fdpb)Cl, Pt(dpb)Cl, Pt(dpb)I and cis-Pt with 1JNX, 1X2J, 2VFJ, 4J80 and 4ZQK target proteins. As can be seen from the obtained data in Table 4, the binding affinity of Pt(F_2dpb)Cl, Pt(Fdpb)Cl, Pt(dpb)Cl and Pt(dpb)I to 1JNX, 1X2J and 4ZQK is higher than cis-Pt. Therefore, these complexes can be preferred to the cis-Pt complex in breast and lung cancer treatment. The interaction energies of Pt(F_2dpb)Cl, Pt(Fdpb)Cl, Pt(dpb)Cl and Pt(dpb)I with 2VFJ target protein is smaller than the interaction energies of cis-Pt with 2VFJ. This indicate that these complexes efficiency on the ovarian tumor may not as effective as cis-platinum. The investigated all complexes exhibit the highest activity with the 1X2J target protein. Therefore, the binding poses of Pt(F_2dpb)Cl, Pt(Fdpb)Cl, Pt(dpb)Cl and Pt(dpb)I complexes with 1X2J, 1X2J, 2VFJ, 4J80 and 4ZQK target protein are given in Figs. 5–9, respectively.

Secondary chemical interactions (H-bond, Polar, Hydrofobic, pi-pi, Halogen-bond) between the chemical species examined in molecular docking studies and the determined target proteins are very important. This situation is very useful in the field of bioinformatics. It can correct the defective amino acid part of the cancer cell line that constitutes the structural characterization. Although the complexes have similar molecular structures, they interact with different amino acid residues of the target proteins. Moreover, due to the various secondary chemical interactions that occur, differences in energy also arise. The types of interactions that are highly bioinformatically important and the different amino acid residues that interact are presented in Tables 8–12.

3.7. Emission spectrum analysis

Excited state geometry optimization was performed at M062X/CEP-31G level to calculate the emission spectrum. Then, using a TD-DFT, emission spectra of the first six excited states were calculated on S1 optimized structures. Relevant emission parameters for better readability are summarized in Table 13. In addition, the assignments of the transitions seen in the calculations have been given in table.

As seen in Table 13, the Pt(F_2dpb)Cl complex has the lowest emission wavelength (375 nm). Another low emission wavelength is 379 nm for the Pt(Fdpb)Cl complex. There is a blue shift with the addition of electronegative fluorine atoms to the structure. The highest emission wavelength (386 nm) belongs to the Pt(dpb)I complex. Adding iodine to the complex instead of chlorine shifted the

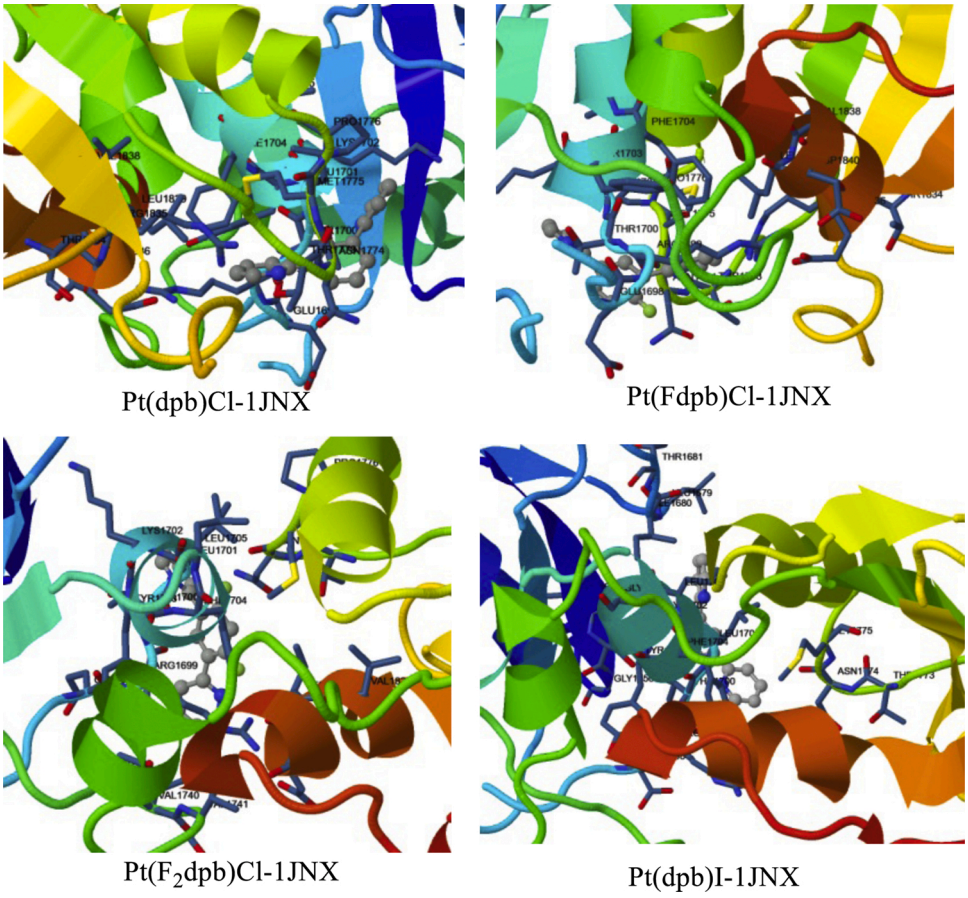

Fig. 5. The binding modes of Pt(dpb)Cl, Pt(Fdpb)Cl, Pt(F_2dpb)Cl, and Pt(dpb)I with 1JNX.

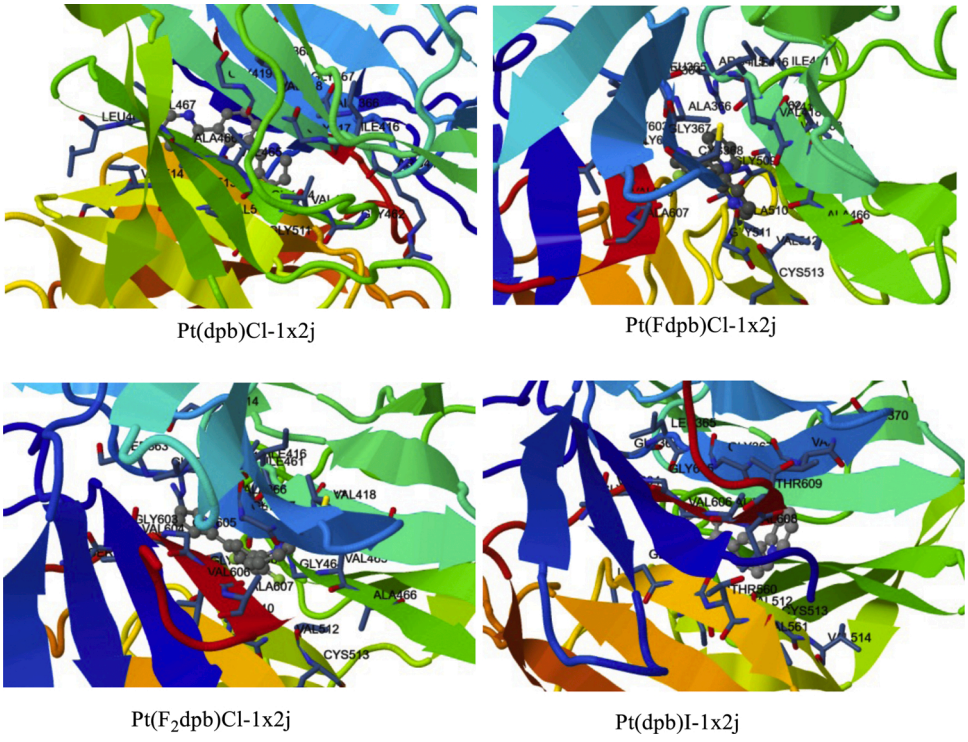

Fig. 6. The binding modes of Pt(dpb)Cl, Pt(Fdpb)Cl, Pt(F_2dpb)Cl, and Pt(dpb)I with 1X2J.

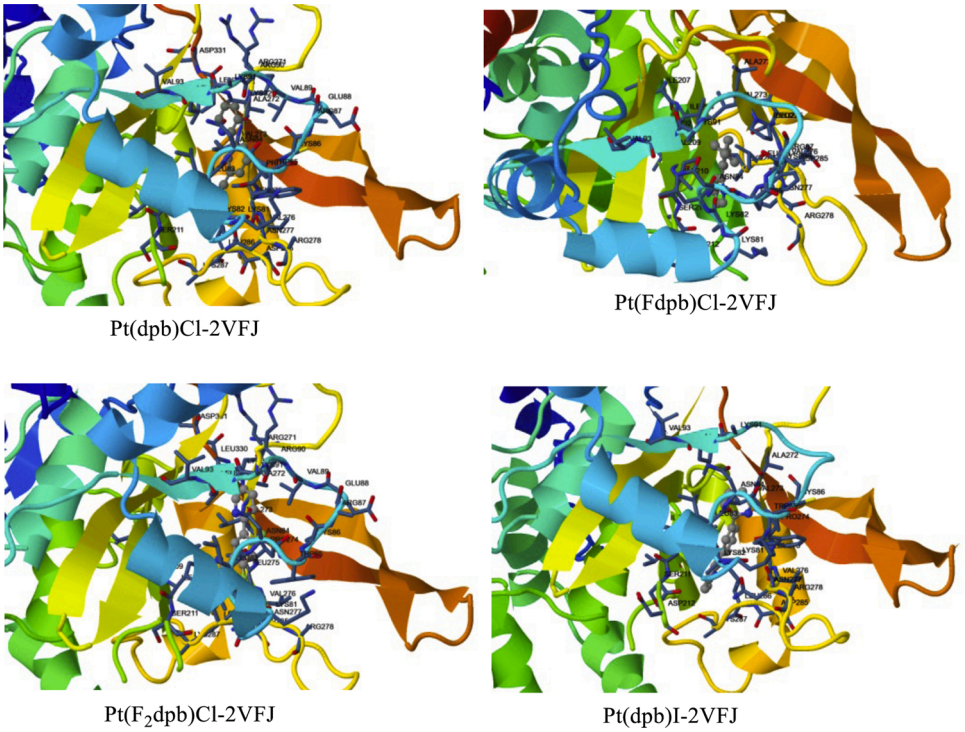

Fig. 7. The binding modes of Pt(dpb)Cl, Pt(Fdpb)Cl, Pt(F_2dpb)Cl, and Pt(dpb)I with 2VFJ.

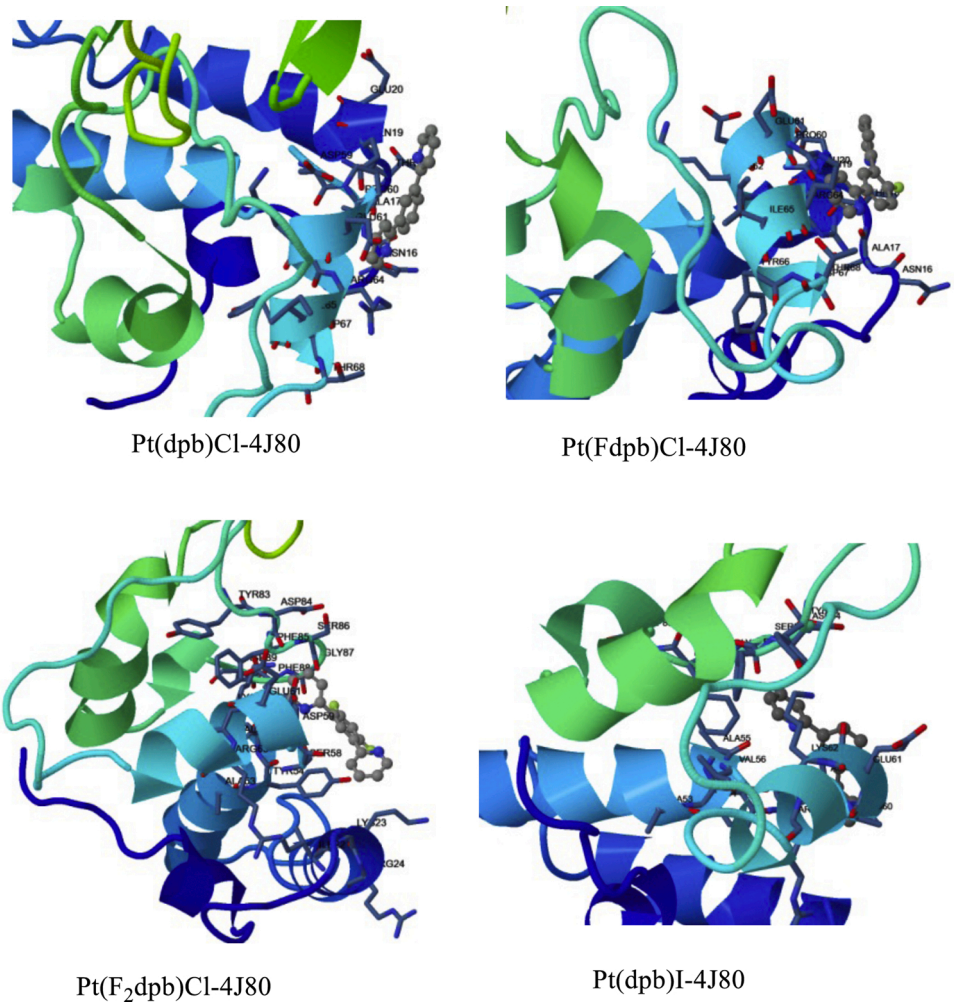

Fig. 8. The binding modes of Pt(dpb)Cl, Pt(Fdpb)Cl, Pt(F_2dpb)Cl, and Pt(dpb)I with 4J80.

emission wavelength slightly towards red. Thus, it can be said that the complexes are capable of emitting blue-green. Table 13 shows the transitions with the highest oscillatory forces. Emission peaks with low transition energy at high wavelengths allow HOMO-→LUMO transitions. High-energy transitions are from HOMO to low-energy orbital and from LUMO to high-energy orbital. The wavelengths obtained from the emission spectra show a similar tendency due to the small structural difference [44].

3.8. OLED properties

Many materials such as organic light emitting diodes (OLEDs) can be designed with computational chemistry methods. Fundamentally, used compounds in OLED structure have been classified as electron-transporting layers (ETL), hole-transporting layers (HTL) and emissive layers (EL) [45,46]. In addition to these layers, there are electron injection layer (EIL), electron blocking layer (EBL), hole injection layer (HIL), and hole blocking layer (HBL) between cathode and anode. EL materials are found between ETL and HTL materials and emit light from red to blue depending on the wavelength of the emission. N,N'-diphenyl-*N*,N'-bis(3-methylphenyl)-1, 1′-diphenyl-4,4′-diamine (TPD) and tris(8-hydroxyquinolinato) aluminum(III) (Alq3) are a typical HTL and a ETL material, respectively. While TPD is metal-free molecules, Alq3 is metallated organic molecules.

Charge transfer is a very important parameter to explain the charge bearing property of the molecule in various biological and chemical reactions [47]. Interactions between conjugated pi-systems play an important role in different events such as stabilization of double stranded DNA structure, protein folding, molecular recognition, and drug design [48]. These interactions are of fundamental technological importance for the development of (bio) molecular devices [49–52]. It is especially important for radiotherapy and chemotherapy tools. One of the main parameters considered in this context is the transfer integral parameter, which is included as "t" in simple semi-classical formulations of charge carrier mobility. "t" is directly related to frontier molecular orbitals (highest molecular orbital (HOMO) and lowest empty molecular orbital (LUMO) energy) due to intermolecular interactions [53].

The transfer integral parameter contains two different combinations. The parameters t_e (electron transfer integral) and th (hole

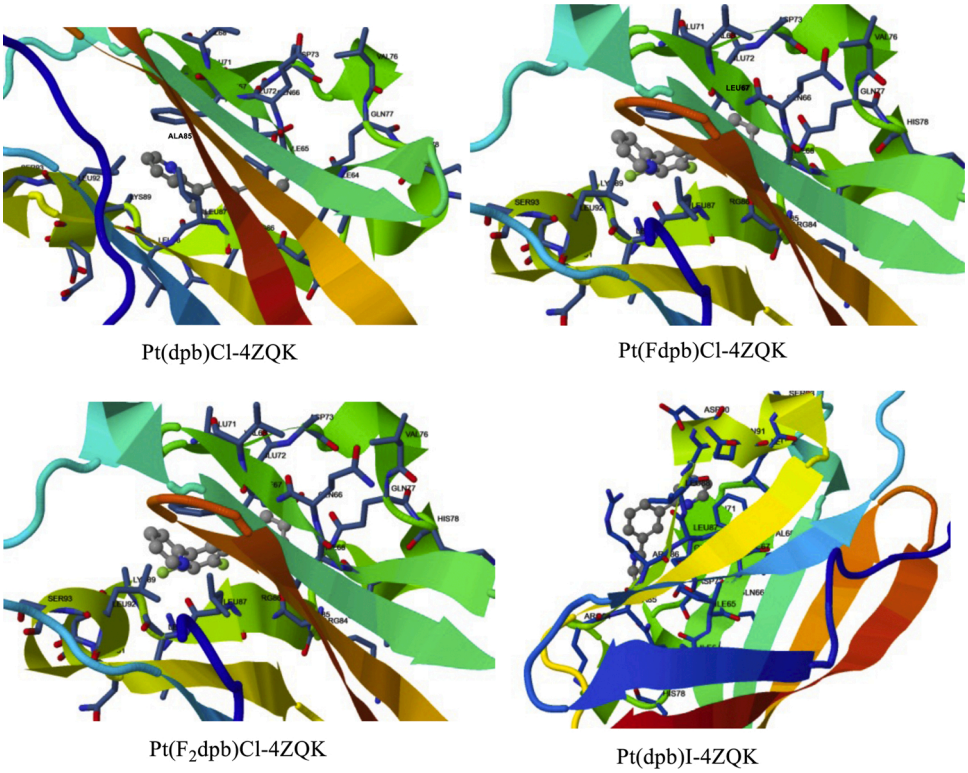

Fig. 9. The binding modes of Pt(dpb)Cl, Pt(Fdpb)Cl, Pt(F_2dpb)Cl, and Pt(dpb)I with 4ZQK.

Table 8
The interaction modes between studied proteins and the selected 1JNX.

Complex	H-bond	Polar	Hydrofobic	pi-pi	Halogen-bond
Pt(dpb)Cl	LEU1701 MET1775 LEU1839	–	–	PHE1704	–
Pt(Fdpb)Cl	LEU1701 MET1775 LEU1839	–		PHE1704	ARG1699
Pt(F_2dpb)Cl	–	ARG1699	VAL1740 MET1775 ILE1680	PHE1704	ASN1774
Pt(dpb)I			LEU1701 LEU1705	–	–

transfer integral) represent the charge movement of the transfer integral in two different regions. t_e (electron transfer integral) and t_h (hole transfer integral) parameters are calculated by the Koopmans theorem (KT) method according to the following equations.

$$t_h = \frac{1}{2}(E_{HOMO} - E_{HOMO-1}) \tag{1}$$

$$t_e = \frac{1}{2}(E_{LUMO+1} - E_{LUMO}) \tag{2}$$

To obtain the transfer integrals "t" parameters, the crystal data of the examined complexes are required. Therefore, t parameters of the complexes will not be examined in this study [54–56].

The charge transfer properties of a molecule can be studied with reorganization energies and Marcus charge transfer theory. The total reorganization energy of the molecule is equal to the sum of internal (λ_{int}) and external (λ_{ext}) reorganization energy. Reorganization energies [57], λ_e and λ_h transfer can be calculated by the following equations:

$$\lambda e = \left(E_0^- - E_-^-\right) + \left(E_-^0 - E_0^0\right) \tag{3}$$

Table 9
The interaction modes between studied proteins and the selected 2VFJ.

Complex	H-bond	Polar	Hydrofobic	pi-pi	Halogen-bond
Pt(dpb)Cl	LYS82 ALA272 ASN277	–	VAL89 LEU92 ILE208 ILE210 VAL273 PRO274 LEU286 LEU330	TRP85	–
Pt(Fdpb)Cl	LYS82 LEU83	TRP85	LEU92 ILE210	–	PRO274
Pt(F_2dpb)Cl	GLY101 ASN189 LEU191	ARG123 TYR252	CYS103 LEU104 MET105 LEU191 ILE196 VAL229	TYR252 PHE257	GLY101 TYR252 HIS255
Pt(dpb)I	LYS82 ASN277	–	LEU92 ILE208 ILE210 VAL273 PRO274 LEU286	–	–

Table 10
The interaction modes between studied proteins and the selected 1X2J.

Complex	H-bond	Polar	Hydrofobic	pi-pi	Halogen-bond
Pt(dpb)Cl	–	–	VAL89 LEU83 ILE210 VAL273 PRO274	ASN84 TRP85	–
Pt(Fdpb)Cl	VAL512	–	CYS513 VAL561	–	VAL418
Pt(F_2dpb)Cl	GLY367 ILE416 VAL418	–	ALA366	–	LEU365 GLY3 VAL604 VAL606
Pt(dpb)I	VAL512	–	ALA466 CYS513 VAL514 ILE559 VAL561	–	–

Table 11
The interaction modes between studied proteins and the selected 4J80.

Complex	H-bond	Polar	Hydrofobic	pi-pi	Halogen-bond
Pt(dpb)Cl	–	ARG63	PRO60	–	–
Pt(Fdpb)Cl	ARG63	–	–	–	–
Pt(F_2dpb)Cl	SER58	TYR54 SER58	–	TYR54 PHE88 PHE85	TYR54 SER86
Pt(dpb)I	SER58	ASP59 LYS62	–	PHE88	–

$$\lambda h = \left(E_0^+ - E_+^+\right) + \left(E_+^0 - E_0^0\right) \tag{4}$$

where E_0^+ is the energy of the cation calculated with the optimized structure of the neutral molecule. E_0^- is the energy of the anion calculated with the optimized structure of the neutral molecule. E_+^+ and E_-^- are the energy of the cation and anion, respectively. E_+^0 is the energy of the neutral molecule calculated at the cationic state. (E_-^0) is the energy of the neutral molecule calculated at the anionic state. E_0^0 is the energy of the neutral molecule at the ground state. With these parameters, the charge transfer rates during electron

Table 12
The interaction modes between studied proteins and the selected 4ZQK.

Complex	H-bond	Polar	Hydrofobic	pi-pi	Halogen-bond
Pt(dpb)Cl	ALA85	ARG86	ILE65 LEU87 LEU92	PHE67	–
Pt(Fdpb)Cl	–	–	LEU87 ILE65	PHE67	LEU87
Pt(F_2dpb)Cl	LEU87	–	LEU87 LEU92	PHE67	LEU87
Pt(dpb)I	LEU87	–	ILE65 LEU87 LEU92	PHE67	–

Table 13
Transition wavelengths, their equivalent values in eV, oscillatory force (f) and assignments of the corresponding transitions in the platinum complexes.

Complex	nm	eV	f	Assignment
Pt(dpb)Cl	175.5	7.15	0.3378	H-10→L+1 (29 %)
	220.9	5.61	0.2656	H-1→L+3 (60 %)
	375.3	3.30	0.1162	HOMO→LUMO (94 %)
Pt(Fdpb)Cl	174.3	7.11	0.4208	H-7→L+2 (20 %)
	269.2	4.67	0.4207	H-1→L+1 (51 %)
	390.1	3.18	0.2178	HOMO→LUMO (92 %)
Pt(F_2dpb)Cl	172.9	7.17	0.1858	H-7→L+2 (20 %)
	247.9	5.00	0.2294	HOMO→L+2 (50 %)
	379.8	3.26	0.7010	HOMO→LUMO (92 %)
Pt(dpb)I	194.2	6.38	0.3564	H-3→L+5 (34 %)
	270.5	4.58	0.1291	HOMO→L+2 (24 %)
	328.8	3.77	0.1190	HOMO→L+1 (74 %)
	398.4	3.11	0.0761	HOMO→LUMO (83 %)

transfer (t_e) and hole transfer (t_h) of the molecule can be calculated by quantum mechanical means with Marcus theory [ruco].

$$K = t^2 \frac{2\pi}{\hbar} \frac{1}{\sqrt{4\pi\lambda k_B T}} exp\left[-\frac{\left(\lambda + \Delta G^0\right)^2}{4\lambda k_B T} \right] \tag{5}$$

where T is the temperature, k_B is the Boltzmann constant. ΔG° is the free energy of the hole transfer reaction (which is zero in the case of a transfer of holes between identical molecules).

In addition, two basic parameters are examined in EIL and HIL materials that determine the ease of charge transfer. These parameters are ionization potentials (IPs) and electron affinities (EAs). In general, lower IP and higher EA mean better hole and electron transport. In other words, smaller IP (larger EA) values indicate easier injection of holes from the transport layer of the holes (electrons) to the emitter layers. [58] Ionization potential (IP_a), vertical ionization potential (IP_v), adiabatic electron affinity (EA_a) and vertical electron affinity (EA_v) are calculated as follows.

$$IP_a = E_+ - E_0^0 \tag{6}$$

$$IP_v = E_0^+ - E_0^0 \tag{7}$$

$$EA_a = E_0^0 - E_- \tag{8}$$

$$EA_v = E_0^0 - E_0^- \tag{9}$$

Table 14
Calculated reorganization energies (in eV) the adiabatic and vertical ionization potentials (IPa/IPv) and electron affinities (EAa/EAv) (in eV) for the platinum complexesc.

Complex	IP_a	IP_v	EA_a	EA_v	λ_e	λ_h
Pt(dpb)Cl	0.2739	0.2799	0.0319	0.0267	0.18	0.15
Pt(Fdpb)Cl	0.2815	0.3088	0.0372	0.0312	0.18	0.18
Pt(F_2dpb)Cl	0.2889	0.2958	0.0401	0.0327	0.16	0.13
Pt(dpb)I	0.2633	0.2909	0.0354	0.0301	0.17	0.10

Here, E_0^- (E_0^+) is the energy of the anion (cation) calculated with the optimized structure of the neutral molecule. E_- (E_+) is the energy of the anion (cation) calculated with the optimized anion (cation) structure [59].

The calculated values of the reorganization energy, the adiabatic and vertical ionization potentials (IP_a/IP_v) and electron affinities (EA_a/EA_v) (in eV) for the complexes examined are listed in Table 14.

In literature, the Alq3 and TPD compounds as the typical ETL and HTL materials have been used as a comparison substance. Also, the electron reorganization energy of Alq3 at 0.276 eV [60] and the hole reorganization energy of TPD at 0.290 eV were reported [61].

The electron and hole reorganization energies of the Pt(dpb)Cl, Pt(Fdpb)Cl, Pt(F_2dpb)Cl and Pt(dpb)I complexes are calculated at 0.18, 0.18, 0.16, 0.17 and 0.15, 0.18, 0.13, 0.10 eV, respectively. In that case, the platinum complexes may be a suitable ETL molecule because its λe values are smaller than that of Alq3. Additionally, it is seen that λh values of the platinum complexes are considerably smaller than that of TPD. Therefore, it can also be a perfect HTL material.

Besides, according to the data in Table 2, Pt(dpb)Cl, Pt(Fdpb)Cl, Pt(F_2dpb)Cl and Pt(dpb)I complexes examined have the lowest IP and EA values in the gas phase. EA values are not high. Therefore, platinum complexes are considered to be an excellent material for HIL.

4. Conclusion

Pt(F_2dpb)Cl, Pt(Fdpb)Cl, Pt(dpb)Cl and Pt(dpb)I complexes were optimized with using HF and DFT (B3LYP and M062X) methods in combining with CEP-4G, CEP-31G, CEP-12G, LANL2DZ, LANL2MB, and SDD basis sets. According to the determined coefficient of R^2, it was found that M062X/CEP-31G is the best level of set. FTIR and ^{13}C-NMR spectrocpic values of studied complexes obtained and interpreted in detail. Platinum complexes, which are important with their anti-cancer properties were docked with molecular simulation against breast, ovarian, colon, pancreatic, lung and melanoma cancer cell lines. The investigated complexes showed the highest inhibitory activity against the breast cancer cell line. We concluded that, after evaluete all theoretical results, the title complexes can be considered as an anticancer drugs. The complexes studied exhibit effectively blue-green light emission capability. Finally, the investigated complexes found to be a good candidate for ETL, HTL and HIL material.

Declaration of Competing Interest

The authors report no declarations of interest.

Acknowledgement

This study was derived from Huner Hama Khalid's MSc Thesis.

References

[1] H. Shi, G.J. Clarkson, P.J. Sadler, Dual action photosensitive platinum (II) anticancer prodrugs with photoreleasable azide ligands, Inorganica Chim. Acta 489 (2021) 230–235.
[2] E. Shaili, Platinum anticancer drugs and photochemotherapeutic agents: recent advances and future developments, Sci. Prog. 97 (1) (2014) 20–40, 2019.
[3] X. Ai, J. Mu, B. Xing, Recent advances of light-mediated theranostics, Theranostics 6 (13) (2016) 2439.
[4] Y. Song, Y. Li, Y. Zhang, L. Wang, Z. Xie, Self-quenching synthesis of coordination polymer pre-drug nanoparticles for selective photodynamic therapy, J. Mater. Chem. B 7 (48) (2019) 7776–7782.
[5] B. Maity, S. Gadadhar, T.K. Goswami, A.A. Karande, A.R. Chakravarty, Photo-induced anticancer activity of polypyridyl platinum (II) complexes, Eur. J. Med. Chem. 57 (2012) 250–258.
[6] K.L. Haas, K.J. Franz, Application of metal coordination chemistry to explore and manipulate cell biology, Chem. Rev. 109 (10) (2009) 4921–4960.
[9] A. Iwakiri, Y. Konno, K. Shinozaki, Determination of excimer emission quantum yield of Pt (dpb) Cl (dpbH= 1, 3-di (2-pyridyl) benzene and its analogues in solution, J. Lumin. 207 (2019) 482–490.
[10] R. Dennington II, T. Keith, J. Millam, GaussView 5.0, Wallingford, CT, 2009.
[11] Gaussian09, R.A, M.J. Frisch, G.W. trucks, H.B. Schlegel, G.E. Scuseria, M.A. Robb, J.R. Cheeseman, G. Scalmani, V. Barone, B. Mennucci, G.A. Petersson, et al., Gaussian, Inc., Wallingford CT, vol. 121, 2009, pp. 150–166.
[12] M. Frisch, G. Trucks, H. Schlegel, G. Scuseria, M. Robb, J. Cheeseman, G. Scalmani, V. Barone, B. Mennucci, G. Petersson, J., and Fox, DJ: Gaussian 09, Revision B. 01, Gaussian Inc, Wallingford CT, 2010.
[13] J.C. Slater, A simplification of the Hartree-Fock method, Phys. Rev. 81 (3) (1951) 385.
[14] A.D. Becke, Perspective: Fifty years of density-functional theory in chemical physics, J. Chem. Phys. 140 (18) (2014), 18A301.
[15] C. Lee, W. Yang, R.G. Parr, Development of the Colle-Salvetti correlation-energy formula into a functional of the electron density, Phys. Rev. B 37 (2) (1988) 785.
[16] Y. Zhao, D.G. Truhlar, The M06 suite of density functionals for main group thermochemistry, thermochemical kinetics, noncovalent interactions, excited states, and transition elements: two new functionals and systematic testing of four M06-class functionals and 12 other functionals, Theor. Chem. Acc. 120 (1–3) (2008) 215–241.
[17] H. Gao, Theoretical studies of molecular structures and properties of platinum (II) antitumor drugs, Spectrochim. Acta - Part A: Mol. Biomol. Spectrosc. 79 (2011) 687–693.
[18] W.P. Oziminski, P. Garnuszek, E. Bednarek, J. Cz Dobrowolski, The platinum complexes with histamine: Pt(II)(Hist)Cl2, Pt(II)(Iodo-Hist)Cl2 and Pt(IV)(Hist) 2Cl2, Inorg. Chim. Acta Rev. 360 (2007) 1902–1914.
[19] L. Zhang, Y. Zhang, H. Tao, X. Sun, Z. Guo, L. Zhu, Theoretical calculation on farinfrared spectra of some palladium(II) and platinum(II) halides: effect of theoretical methods and basis sets, J. Mol. Struct.: Theochem. 617 (2002) 87–97.
[20] D.N. Sathyanarayana, Vibrational Spectroscopy: Theory and Applications, New Age International, 2015.
[21] G. Varsányi, Assignments for Vibrational Spectra of Seven Hundred Benzene Derivatives, Halsted Press, 1974.
[22] J. Mohan, Organic Spectroscopy: Principles and Applications, Alpha Science Int'l Ltd., 2004.

[23] J. Lorenc, Dimeric structure and hydrogen bonds in 2-N-ethylamino-5-metyl-4-nitro-pyridine studied by XRD, IR and Raman methods and DFT calculations, Vib. Spectrosc. 61 (2012) 112–123.
[24] Y. Sharma, Elementary Organic Spectroscopy, Principles and Chemical Application, Chand and Company Ltd, New Delhi, India, 2009.
[25] S. Ramachandran, G. Velraj, FT-IR, FT-Raman spectral analysis and density functional theory calculations studies of 3-chloro-2-nitrobenzyl alcohol, Rom. J. Physiol. 57 (7-8) (2012) 1128–1137.
[26] A. Abkowicz-Bienko, D. Bienko, Z. Latajka, Density functional studies on the two conformers of 2-fluoro-4, 6-dinitrophenol: vibrational assignment based on potential energy distribution, J. Mol. Struct. 552 (1–3) (2000) 165–175.
[27] T. Ardyukoiva, Atlas of Spectra of Aromatic and Heterocyclic Compounds, Nauka Sib otd, Novosibirsk, 1973.
[28] G. Varsányi, Vibrational Spectra of Benzene Derivatives, Elsevier, 2012.
[29] V. Krishnakumar, N. Surumbarkuzhali, S. Muthunatesan, Scaled quantum chemical studies on the vibrational spectra of 4-bromo benzonitrile, Spectrochim. Acta A Mol. Biomol. Spectrosc. 71 (5) (2009) 1810–1813.
[30] G.D. Fleming, R. Koch, M.C. Vallette, Theoretical study of the syn and anti thiophene-2-aldehyde conformers using density functional theory and normal coordinate analysis, Spectrochim. Acta A Mol. Biomol. Spectrosc. 65 (3-4) (2006) 935–945.
[31] A. Ünal, B. Eren, FT-IR, dispersive Raman, NMR, DFT and antimicrobial activity studies on 2-(Thiophen-2-yl)-1H-benzo [d] imidazole, Spectrochim. Acta A Mol. Biomol. Spectrosc. 114 (2013) 129–136.
[32] H.M. Badawi, Structural stability, C–N internal rotations and vibrational spectral analysis of non-planar phenylurea and phenylthiourea, Spectrochim. Acta A Mol. Biomol. Spectrosc. 72 (3) (2009) 523–527.
[33] H. Knicker, G. Almendros, F.J. González-Vila, H.-D. Lüdemann, F. Martin, 13C and 15N NMR analysis of some fungal melanins in comparison with soil organic matter, Org. Geochem. 23 (11-12) (1995) 1023–1028.
[34] J.R. Cheeseman, G.W. Trucks, T.A. Keith, M.J. Frisch, A comparison of models for calculating nuclear magnetic resonance shielding tensors, J. Chem. Phys. 104 (14) (1996) 5497–5509.
[35] M. Frisch, G. Trucks, H. Schlegel, G. Scuseria, M. Robb, J. Cheeseman, V. Zakrzewski, J. Montgomery Jr, R.E. Stratmann, J. Burant, Gaussian 98, Revision A. 7, Gaussian, Inc., Pittsburgh, PA, 1998, p. 12.
[36] S. Erkan, S. Kaya, K. Sayin, D. Karakaş, Structural, spectral characterization and molecular docking analyses of mer-ruthenium (II) complexes containing the bidentate chelating ligands, Spectrochim. Acta A Mol. Biomol. Spectrosc. 224 (2020), 117399.
[37] R.S. Williams, R. Green, J.M. Glover, Crystal structure of the BRCT repeat region from the breast cancer-associated protein BRCA1, Nat. Struct. Biol. 8 (10) (2001) 838–842.
[38] B. Padmanabhan, K.I. Tong, T. Ohta, Y. Nakamura, M. Scharlock, M. Ohtsuji, et al., Structural basis for defects of Keap1 activity provoked by its point mutations in lung cancer, Mol. Cell 21 (5) (2006) 689–700.
[39] D. Komander, D. Barford, Structure of the A20 OTU domain and mechanistic insights into deubiquitination, Biochem. J. 409 (1) (2008) 77–85.
[40] T.R. Barends, R.W. Brosi, A. Steinmetz, A. Scherer, E. Hartmann, J. Eschenbach, et al., Combining crystallography and EPR: crystal and solution structures of the multidomain cochaperone DnaJ, Acta Crystallogr. D Biol. Crystallogr. 69 (8) (2013) 1540–1552.
[41] K.M. Zak, R. Kitel, S. Przetocka, P. Golik, K. Guzik, B. Musielak, et al., Structure of the complex of human programmed death 1, PD-1, and its ligand PD-L1, Structure 23 (12) (2015) 2341–2348.
[42] D. Ritchie, T. Orpailleur, Hex 8.0. 0 User Manual. Protein Docking Using Spherical Polar Fourier Correlations Copyright C, 1996.
[43] Z. Bikadi, E. Hazai, Application of the PM6 semi-empirical method to modeling proteins enhances docking accuracy of AutoDock, J. Cheminform. 1 (1) (2009) 15, 2015.
[44] F. Cervantes-Navarro, D. Glossman-Mitnik, DFT study of the effect of substituents on the absorption and emission spectra of Indigo, Chem. Cent. J. 6 (1) (2012) 70.
[45] J.H. Kim, R.E. Triambulo, J.W. Park, Effects of the interfacial charge injection properties of silver nanowire transparent conductive electrodes on the performance of organic light-emitting diodes, J. Appl. Phys. 121 (10) (2017), 105304.
[46] J. Zhao, X. Chen, Z. Yang, T. Liu, Z. Yang, Y. Zhang, et al., Highly-efficient doped and nondoped organic light-emitting diodes with external quantum efficiencies over 20% from a multifunctional green thermally activated delayed fluorescence emitter, J. Phys. Chem. C 123 (2) (2018) 1015–1020.
[47] M. Melander, E.O. Jónsson, J.J. Mortensen, T. Vegge, J.M. García Lastra, Implementation of constrained DFT for computing charge transfer rates within the projector augmented wave method, J. Chem. Theory Comput. 12 (11) (2016) 5367–5378.
[48] S. Erkan, Activity of the rocuronium molecule and its derivatives: a theoretical calculation, J. Mol. Struct. 1189 (2019) 257–264.
[49] S. Wu, M.T. González, R. Huber, S. Grunder, M. Mayor, C. Schönenberger, M. Calame, Molecular junctions based on aromatic coupling, Nat. Nanotechnol. 3 (9) (2008) 569.
[50] N. Nerngchamnong, L. Yuan, D.C. Qi, J. Li, D. Thompson, C.A. Nijhuis, The role of van der Waals forces in the performance of molecular diodes, Nat. Nanotechnol. 8 (2) (2013) 113.
[51] L. Venkataraman, J.E. Klare, C. Nuckolls, M.S. Hybertsen, M.L. Steigerwald, Dependence of single-molecule junction conductance on molecular conformation, Nature 442 (7105) (2006) 904–907.
[52] Z.L. Cheng, R. Skouta, H. Vazquez, J.R. Widawsky, S. Schneebeli, W. Chen, et al., In situ formation of highly conducting covalent Au–C contacts for single-molecule junctions, Nat. Nanotechnol. 6 (6) (2011) 353.
[53] J. Cornil, D. Beljonne, J.P. Calbert, J.L. Brédas, Interchain interactions in organic π-conjugated materials: impact on electronic structure, optical response, and charge transport, Adv. Mater. 13 (14) (2001) 1053–1067.
[54] S.H. Wen, A. Li, J. Song, W.Q. Deng, K.L. Han, W.A. Goddard III, First-principles investigation of anistropic hole mobilities in organic semiconductors, J. Phys. Chem. B 113 (26) (2009) 8813–8819.
[55] S. Chai, S.H. Wen, J.D. Huang, K.L. Han, Density functional theory study on electron and hole transport properties of organic pentacene derivatives with electron-withdrawing substituent, J. Comput. Chem. 32 (15) (2011) 3218–3225.
[56] W.Q. Deng, L. Sun, J.D. Huang, S. Chai, S.H. Wen, K.L. Han, Quantitative prediction of charge mobilities of π-stacked systems by first-principles simulation, Nat. Protoc. 10 (4) (2015) 632.
[57] M.S. Stark, Epoxidation of alkenes by peroxyl radicals in the gas phase: structure– activity relationships, J. Phys. Chem. A 101 (44) (1997) 8296–8301.
[58] J. Gao, J. Li, X. Li, D. Han, P. Guo, X. Zhu, X. Shang, Theoretical investigation on the effect of the modification of 2-phenylpyridine ligand on the photophysical properties for a series of iridium (III) complexes with carbazate ancillary ligands, J. Lumin. 209 (2019) 365–371.
[59] A. Üngördü, Electronic, optical, and charge transfer properties of porphyrin and metallated porphyrins in different media, Int. J. Quantum Chem. 120 (6) (2020) e26128.
[60] A. Lukyanov, C. Lennartz, D. Andrienko, Amorphous films of tris (8-hydroxyquinolinato) aluminium: force-field, morphology, and charge transport, Physica Status Solidi (A) 206 (12) (2009) 2737–2742.
[61] N.E. Gruhn, D.A. da Silva Filho, T.G. Bill, M. Malagoli, V. Coropceanu, A. Kahn, J.L. Brédas, The vibrational reorganization energy in pentacene: molecular influences on charge transport, J. Am. Chem. Soc. 124 (27) (2002) 7918–7919.

Refine Your Search Results

Optik

Search

Sort By: Title (A-Z)

Search Results

Found 1 results (Page 1) Share These Results

Exact Match Found

OPTIK

Publisher: ELSEVIER GMBH , HACKERBRUCKE 6, MUNICH, GERMANY, 80335

ISSN / eISSN: 0030-4026 / 1618-1336

Web of Science Core Collection: Science Citation Index Expanded

Additional *Web of Science* Indexes: Current Contents Engineering, Computing & Technology | Current Contents Physical, Chemical & Earth Sciences | Essential Science Indicators

Share This Journal View profile page

Items per page: 10 1 – 1 of 1

Results: 1
(from Web of Science Core Collection)

You searched for: TITLE: (Halogens effect on spectroscopy, anticancer and molecular docking studies for platinum complexes) ...More

Create an alert

Refine Results

Search within results for...

Publication Years
- 2021 (1)

Refine

Web of Science Categories
- OPTICS (1)

Refine

Document Types
- ARTICLE (1)

Refine

Organizations-Enhanced
- CUMHURIYET UNIVERSITY (1)
- FIRAT UNIVERSITY (1)

more options / values...

Refine

Funding Agencies

Authors

Source Titles

View all options

For advanced refine options, use
Analyze Results

Sort by: Date Times Cited Usage Count Relevance More

1 of 1

Select Page Export... Add to Marked List

Analyze Results
Create Citation Report

1. **Halogens effect on spectroscopy, anticancer and molecular docking studies for platinum complexes**

By: Khalid, Hunar Hama; Erkan, Sultan; Bulut, Niyazi

OPTIK Volume: 244 Article Number: 166324 Pu

Times Cited: 1
(from Web of Science Core Collection)

View Abstract

Select Page Export... Add to Marked List

Sort by: Date Times Cited Usage Count Relevance

Show: 10 per page

1 records matched your query of the 78,725,508 in the data limits you s

OPTIK

Impact Factor

2.443	1.955
2020	*5 year*

JCR ® Category	*Rank in Category*	*Quartile in Category*
OPTICS	47 of 99	Q2

Data from the 2020 edition of Journal Citation Reports

Publisher
ELSEVIER GMBH, HACKERBRUCKE 6, 80335 MUNICH, GERMANY

ISSN: 0030-4026
eISSN: 1618-1336

Research Domain
Optics

Close Window